

BRI3L: A BRIGHTNESS ILLUSION IMAGE DATASET FOR IDENTIFICATION AND LOCALIZATION OF REGIONS OF ILLUSORY PERCEPTION

Aniket Roy¹, Anirban Roy², Soma Mitra³, Kuntal Ghosh⁴

¹Johns Hopkins University, ²SRI International, ³CDAC Kolkata, ⁴Indian Statistical Institute

ABSTRACT

Visual illusions play a significant role in understanding visual perception. Current methods in understanding and evaluating visual illusions are mostly deterministic filtering based approach and they evaluate on a handful of visual illusions, and the conclusions therefore, are not generic. To this end, we generate a large-scale dataset of 22,366 images (BRI3L: BRightness Illusion Image dataset for Identification and Localization of illusory perception) of the five types of brightness illusions and benchmark the dataset using data-driven neural network based approaches. The dataset contains label information - (1) whether a particular image is illusory/non-illusory, (2) the segmentation mask of the illusory region of the image. Hence, both the classification and segmentation task can be evaluated using this dataset. We follow the standard psychophysical experiments involving human subjects to validate the dataset. To the best of our knowledge, this is the first attempt to develop a dataset of visual illusions and benchmark using data-driven approach for illusion classification and localization. We consider five well-studied types of brightness illusions: 1) Hermann grid, 2) Simultaneous Brightness Contrast, 3) White illusion, 4) Grid illusion, and 5) Induced Grating illusion. Benchmarking on the dataset achieves 99.56% accuracy in illusion identification and 84.37% pixel accuracy in illusion localization. The application of deep learning model, it is shown, also generalizes over unseen brightness illusions like brightness assimilation to contrast transitions. We also test the ability of state-of-the-art diffusion models to generate brightness illusions. We have provided all the code, dataset, instructions etc in the github repo: <https://github.com/aniket004/BRI3L>

Index Terms— visual illusion, perception

1. INTRODUCTION

Brightness illusions are a special and well explored class of visual illusions where the perceived brightness of a region is different from the actual brightness in the image. A few instances of the brightness illusion and the corresponding illusory regions are shown in Fig. 1. Brightness illusions can be classified into three major classes according to changes in directions of the brightness: 1) brightness-contrast, 2)

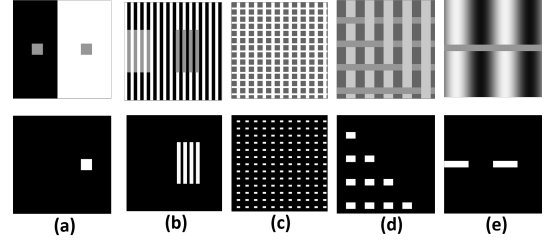


Fig. 1. Examples of brightness illusion (top row) and the binary masks corresponding to certain illusory regions in the image (bottom row): (a) simultaneous brightness contrast (SBC), (b) White illusion, (c) Hermann grid, (d) grid illusion, (e) grating illusion. The illusory regions correspond to the illusory phenomenon such as apparent false perception of brightness/darkness values based on the context. Our goal is to localize these illusory regions in the illusory images.

brightness-assimilation, and 3) illusory blobs or region illusions [1]. In brightness-contrast illusions, the brightness induction in the test patch occurs in opposite direction to the surrounding luminance such as the simultaneous brightness contrast (SBC) [2] in Fig. 1 (a). In this example, the right test patch looks darker since it is surrounded by brighter background causing a contrast of brightness. In brightness-assimilation illusions, the brightness induction occurs in the same direction such as the White illusion [3] in Fig. 1 (b). In this example, the right test patches look darker while it is surrounded by darker background causing an assimilation of brightness. In the illusory blobs or region illusions, pseudo bright or dark blobs, bands, or contours appear in the image corners such as the Hermann grid [4] as shown in Fig. 1 (c). Some other complex brightness perception illusions like the grid illusion (Fig. 1 (d)) and the grating illusion [5] (Fig. 1 (e)) are also shown.

Localizing illusory regions is important as it helps to identify the nature of illusions and facilitate understanding the reason behind the illusory phenomenon [6, 7, 1]. Localizing illusory regions in a brightness illusion is challenging as the intensity values in the illusory and non-illusory regions can be exactly the same (Fig. 1(a) top). Though these regions appear to be of different brightness values to humans, it can be difficult for image processing approaches to differentiate them. For example, various threshold-based illusion segmentation

approaches, e.g., Otsu [8], can not differentiate the illusory regions from the non-illusory regions as the intensity values are the same in those regions.

Traditionally, spatial filtering based approaches are employed to localize illusions in images [9, 10, 1] where hand-crafted filters, such as the Difference of Gaussians (DOG), Laplacian of a Gaussian (LOG), and their more contemporary versions (ODOG, LODOG, FLODOG) [10] are designed to localize illusory regions in the images. However, as noted in some papers [11, 6], these filtering based approaches are inadequate in explaining complex versions of brightness illusions. Gilchrist et al. [11] refer the spatial filtering based models as intrinsic image based models and suggest an alternative approach for brightness perception based on anchoring theory. Recently, Gomez et. al. [12] show that training a shallow neural network on low-level tasks (e.g., image denoising) can be effective to explain visual illusions. However, their approach does not generalize across various gray-scale illusions such as the higher spatial frequency induced assimilation illusions [12].

To address the above-mentioned challenges, we introduce a large-scale dataset of five types of commonly used brightness illusion with the annotated illusion regions (Fig. 1 (bottom row)). Then we benchmark the dataset (BRI3L: BRightness Illusion Image dataset for Identification and Localization of illusory perception) using a data-driven neural-network approach to distinguishing illusions from non-illusions and localize the illusory regions in the illusion images. Specifically, given an image, we identify if the image represents an illusion and localize the illusory regions in the image. We consider a ResNet (a neural network with residual connections) [13] to classify the illusion images from non-illusion images. For illusion localization, we consider a U-Net (an encoder-decoder neural network) [14] to segment the illusory regions in illusion images. Moreover, we show that neural networks trained on a specific type of illusions, can generalize to unseen types of illusions.

Our main contributions include:

- We introduce a large-scale dataset of 22,366 images containing five types of brightness illusions. We annotate each image with the binary mask corresponding to illusory regions in the image. We validate the dataset by conducting standard psychophysical experiments involving human experts. The dataset and training details are provided in the supplementary material.
- A data-driven neural network-based approach to identify brightness illusions and localize the illusory regions. To the best of our knowledge, this is the first attempt to consider a data-driven approach for illusion localization.
- Unlike the common filtering based approaches, our approach is generalizable to novel types of illusions. Moreover, we can also address the intriguing transition

from brightness contrast to assimilation.

- We consider a perception-inspired structural similarity loss suitable for illusion localization. Our experiments show that this loss is crucial for illusion localization.
- This work reports the first attempt to investigate the ability of state-of-the-art diffusion models to generate brightness illusions.

2. PRIOR WORK

The approaches for illusion analysis can be broadly classified into two categorized as follows.

Filtering based approaches. There exists a plethora of filtering based approaches for illusion understanding that are mainly inspired by the visual pathway and brain structure and try to establish a one-to-one mapping with some of the biological structure of the visual system to explain several classes of brightness illusion [15, 9, 10, 1, 16, 17]. For example, the Oriented Difference of Gaussian (ODOG) model suggests that the input image is filtered with several directional Difference of Gaussian (DOG) filters which is mostly inspired by the Hubel-Wiesel’s experiments in V1 cat and macaque cells [18]. Frequency-specific Locally normalized ODOG (FLODOG) [10] further suggests that the normalization step in ODOG model should be performed locally and in frequency sensitive manner. Similar strategies has been adopted by [1, 19, 20].

Data-driven approaches. In spite of the tremendous success of neural networks in various vision application, some recent studies show that they may not be able to emulate some basic perceptual phenomenon [21]. Therefore, recently a line of research devoted to studying the similarities and differences of biological and machine vision. Kim et al. [22] showed that neural networks trained with natural images for classification exhibit the Gestalt’s law of closure. Benjamin et al. [23] observed that DNNs trained on Imagenet for classification shows orientation bias for geometric illusions similar to human observers. Ward et al. [24] verified that DNN trained for object recognition exhibits geometric Muller-Lyon illusion. Serre et al. [25] designed a deep RNN inspired by the orientation-tilt illusion, which outperforms state-of-the-art contour detection approach. Recently, Watanabe et al. [26] train a self-supervised predictive network (Pred-Net) for video prediction and apply it to successfully predict the illusory motion of the rotating snake illusion. Gomez et. al. [12] show that a network on low-level tasks, such as denoising, deblurring, can explain the response of visual illusions. In a subsequent work [27], a GAN is employed to generate visual illusions by constructing background for a target with aid of an illusion discriminator. Williams et al. [28] also consider GANs for generating visual illusions, however, they are unable to fool human vision. Recently, Hirsch et al. [29] also used flow-based methods to generate color visual images.

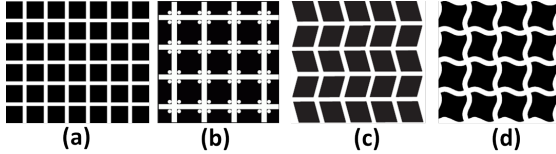


Fig. 2. (a): Actual Hermann grid; Weak or non-illusion variants of Hermann grid by (b) inserting blobs, (c) and (d) introducing non-linearity. [30]

3. BRI3L: A BRIGHTNESS ILLUSION IMAGE DATASET

3.1. Dataset generation

To facilitate research on illusion understanding, we create a large-scale dataset containing five types of brightness illusions: 1) Hermann grid, 2) SBC, 3) White illusion, 4) grating, 5) Grid illusion and non-illusion variants.

Illusion images We synthetically generate illusion images for each of these five classes of brightness illusions as shown in Fig. 1. Each image is annotated with the binary segmentation mask corresponding to illusory regions in the image. The dataset is created by considering several variations of illusion-related parameters including patch and grid width, height, and intensity values. The dataset contains 22366 illusion images of size 256×256 consisting of 4160 SBC illusions, 637 White illusions, 1024 Hermann grid illusions, 6350 induced grating illusions, and 10195 upper and lower grid illusions. The grayscale values are varied in ranges $\{100, 150, 200, 250\}$ grayscale values, and the aspect ratio ranges of $\{0.2, 0.4, 0.8\}$ for SBC and White illusions. The spatial frequency of grating illusions vary from 4-50 cycles per degrees. More examples are provided in the supplementary material.

Non-illusion images To distinguish between illusion vs non-illusion, non-illusion samples are also required. We generate 1149 non-illusion images that are carefully created by slightly modifying the image to make the illusory effect disappear [30, 31]. Some of the non-illusions are shown in Fig. 2. To generate such non-illusion variants, we consider standard techniques [30, 31] such as dot-insertion (Fig. 2 (b)), changing orientation (Fig. 2 (c)), and applying non-linear transformation (Fig. 2 (d)). Since there are only limited number of such modifications that make the illusory effects disappear, the number of non-illusion images are comparatively small. Note that a large number of natural images can be considered to be non-illusion images but those are significantly different from illusion images. Our non-illusion images are visually similar to illusion images and thus, identifying illusion images is not a trivial task. The dataset is validated by conducting standard psychophysical experiments supervised by domain experts as described below.

3.2. Psychophysical experiment for dataset validation.

Since the illusory effect is subjective in nature, Psychophysical experiments are designed to measure the illusory effect quantitatively and can also judge the direction of the illu-

Table 1. Quantitative Illusory Reduction for different illusions

Subject	SBC Illusion	White Illusion	Grating Illusion	Grid Illusion
subject 1	35.03	49.22	27.11	32.95
subject 2	50.47	69.24	38.79	41.71
subject 3	44.21	62.15	47.97	49.63
subject 4	47.55	58.39	33.37	46.3
subject 5	45.46	49.63	37.12	31.28
subject 6	32.95	42.54	26.69	29.61
subject 7	45.88	52.14	30.45	30.45
Avg. illusory effect	43.08	54.76	34.50	37.42

sory effect. We perform psychophysical experiments to validate the dataset using the standard two alternate forced-choice (2AFC) experiment [32, 33].

Experimental Setup A psychophysical experiment consists of a number of components like stimulus (comparator and standard), task, method, analysis and measure. Two types of procedures exist in psychophysical experiments. In the first type, the comparator is displayed on the computer screen and the observer has to adjust the contrast within a predefined limit to achieve the perceivable intensity as compared with the standard. For this type of procedure, the task and the method are collectively termed as ‘method of adjustment’. Nowadays the preferred approach is to display the comparator and standard in a random fashion on a computer screen for a short duration of time. The observer has to decide the relative brightness of the comparator with respect to that of the standard and indicate his/her choice by pressing a key. This is known as 2 Alternate Forced Choice (2AFC) experiment [32].

In this experiment, seven human subjects, four men and three women (all in age range of 23 to 68 and in perfect health condition) in our case, visually compare the brightness of two target patches: a standard (‘S’) and a comparator (‘C’). We conduct a 2AFC experiment for comparing the brightness between the standard and the comparator in order to measure the illusory enhancement or illusory reduction. The subjects are instructed to provide their feedback by pressing the key marked ONE when the comparator appeared to be brighter than the standard and the key marked as TWO, otherwise. Comparing the ‘comparator’ with the ‘standard’ under various contexts help us identifying the effect of illusion. The comparator (as shown in Fig. 5) is an intensity-based illusion and it is selected from four types of brightness illusions: SBC, White illusion, gratings, and grid illusions. For the psychophysical experiment, we randomly choose 700 SBC, 400 White illusions, 400 grid illusions, and 400 grating illusions. Since the illusory dots are not physically present in the Hermann grid illusions, they can not be validated using this experiment.

Psychometric Results The psychometric curves (using seven observers) for SBC, White illusion, gratings illusion and lower grid illusion are provided in Fig. 3. We have also done similar psychophysical experiments for White, grating and grid illusion and the illusory reduction is shown in Table. 1, which shows similar trend holds for other illusions and we observe similar psychometric curve for White, grating and grid illusion as well. Illusory decrement indicates the quanti-

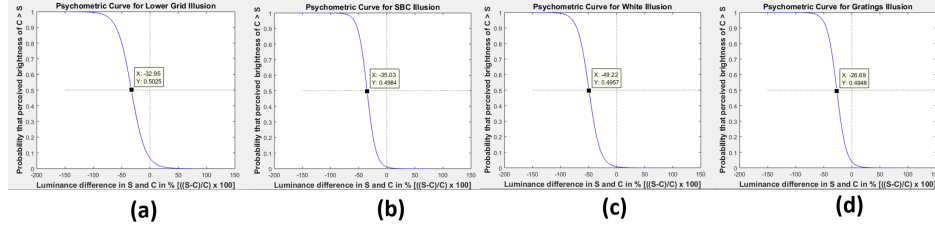


Fig. 3. Psychometric curve for (a) Lower grid, (b) SBC, (c) White illusion, (d) Grating illusion taken from the generated dataset. This indicates the probability that the perception agrees with the reality as a function of the real difference in luminance between the standard (S) and the comparator (C). The illusory reduction for Grating, White illusion, SBC, Lower grid are 26.69, 49.22, 35.03 and 32.95 respectively.

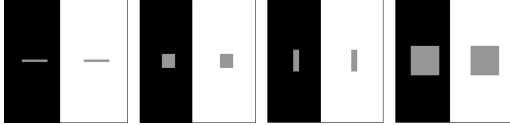


Fig. 4. Different types of SBC illusions selected as the comparator. The intensity level of the target is always 150. However the length and width of the target varies widely.

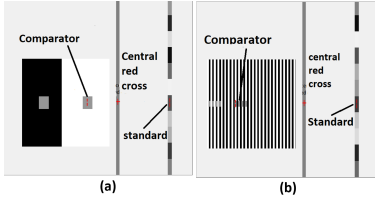


Fig. 5. Experimental setup for two-alternative forced-choice experiment for (a) SBC and (b) White illusion. Darker regions (red marked) are compared with the standard randomly multiple times to get the data.

tative measure of perceived darkness. For example, given the standard grayscale value to be 150, illusory reduction of 32.95 indicates that the target is perceived to be grayscale value of 117.05 and looks darker. The illusory reduction of the same intensity comparator of grayscale value 150 for White illusion is maximum (49.22), for gratings illusion is minimum (27.11), and it lies within this maximum and minimum limit for SBC (35.03) and Lower-grid illusion (32.95) as shown in Fig. 3. These psychophysical experiments statistically validate the dataset. A detailed description of the experimental setup is provided in the supplementary material.

4. TASKS: ILLUSION IDENTIFICATION, LOCALIZATION AND GENERATION

1. Illusion identification. Illusion identification is posed as a binary decision problem to identify whether an image is a brightness illusion or not. Although we have a relatively large collection of illusion images, non-illusion images are relatively scarce. To combat the nuisance of data imbalance, we have performed data augmentation since any linear transformation on a non-illusion image tends to be a non-illusion itself. Recall that we only consider carefully created non-illusion images which are visually similar to illusion images instead of widely available natural images (Fig. 2). For classification, we consider three widely explored variants of CNNs:

1) AlexNet [34] which is a five-layer CNN, 2) Resnet-18 [13] which is an 18-layer CNN with residual connections between the layers, and 3) SqueezeNet [35] which is designed for low-capacity devices with very small number of parameters. For training, we use binary cross-entropy loss and stochastic gradient descent optimization with a learning rate of 0.001 and a momentum of 0.9. Details of the networks are provided in the supplemental material.

2. Illusion Localization. We cast illusion localization as a binary segmentation problem, where we localize the region corresponding to perceived darkness in the image. Recall that we follow the convention to localize the perceived *darkness* and the complementary lightness regions can be inferred by matching the intensity value. We consider the UNet [14] for segmentation. The network contains two paths. The first path is the contraction path (as an encoder) which captures the high-level details such as the larger context of the image. The second path is the expanding path (as a decoder) which captures the low-level details such as edges and local textures. This network is suitable for illusion localization as it can capture local brightness variation and observe the local brightness regions in a larger context to perceive the illusion.

For training the segmentation network, along with the commonly used mean square error (MSE) loss, we also consider the structural similarity index metric (SSIM) to capture perceptual similarity. Bovik et al. [36] introduced the SSIM inspired by the fact that human perception is highly adapted to perceive structured information in a scene. We consider a differentiable version of SSIM which is shown to be effective for several low-level tasks including deblurring and denoising [37]. We consider a convex combination of MSE loss (L_{MSE}) and SSIM loss (L_{SSIM}) as the loss function, $L = \alpha L_{MSE} + \beta L_{SSIM}$, where L_{MSE} is mean squared error loss and L_{SSIM} [37] is the SSIM loss. We experimentally set the parameters, $\alpha = 0.4$, $\beta = 0.6$, which produced the best performance (Tab. 5). We consider the Adam optimizer with a learning rate of 0.001 and a batch size of 32 images.

3. Illusion generation using diffusion model. Motivated by the recent success of generative models, we generate illusions using text-to-image [38] and image-to-image diffusion model [39]. To the best of our knowledge, we are first to investigate the ability of generating illusions through diffu-

sion models. We use stable diffusion [38] for both the cases, where text-to-image diffusion model uses “class name” (e.g, Hermann grid illusion, White illusion etc.) as text prompt and image-to-image diffusion model uses both illusion images and text prompt (i.e., class names) as input to generate diverse illusions. Since the diffusion models are not trained on illusion dataset (which practically does not exists earlier), it generates somewhat misleading images (Fig. 6). However, image-to-image diffusion model modifies input illusion images guided by text prompts (i.e., class names), thus generates interesting variants of illusions as shown in Fig. 6. We have tested the generated illusion images using experts and it seems the image-to-image diffusion model generates better illusions than text-to-image diffusion model. In particular, the essence of the brightness illusions are captured properly for SBC, White illusions (as shown in Fig. 6) and qualitatively the rank of quality of generated illusions are as follows: SBC > White illusion > Hermann grid (through observation of experts). To quantify the generative quality of these images, we train a classifier (2 layer MLP on top of ResNet feature extractor) using the text-to-image and image-to-image generated images for each of the five class of illusion and test on the same set of actual illusion images. The classification performance is lower for classifier trained on just text-to-image generated images, but significantly improves when trained on image-to-image generated images as shown in Tab. 3.

5. EXPERIMENTS

We perform the following experiments to evaluate various aspects of our approach: 1) illusion identification, 2) illusion localization, 3) generalization of illusion localization to transition between illusions, and 4) analysis of network layers for the models trained on natural images vs. illusion images. Our dataset and code can be downloaded from the public domain <https://github.com/aniket004/BRI3L>.

Metrics. For illusion identification, we consider *Accuracy*, *F1-score*, *Precision*, *Recall* as metrics and for illusion localization, we consider pixel-wise *F1-score* and *mean Intersection Over Union (mIOU) metric* which is commonly used to evaluate segmentation approaches [14]. We provide the description of the dataset creation in the supplementary material.

1. Illusion identification. We have 22,366 illusion images and 1149 non-illusion images in the dataset. We augment the non-illusion images to create a balanced set for training. We consider common data-augmentation approaches such as random resized cropping, center-cropping, vertical flip, horizontal flip to make around 3000 non-illusions, from which 2000 used for training and 1000 for testing. Then we randomly sample 1000 illusions from all variants of illusions for training and the rest of the images are used for testing. We consider three standard models - AlexNet, ResNet-18, and SqueezeNet. We achieve 99.56% accuracy for illusion identification as shown in Table 2. We also perform illusion classification to correctly classify illusion images into one of

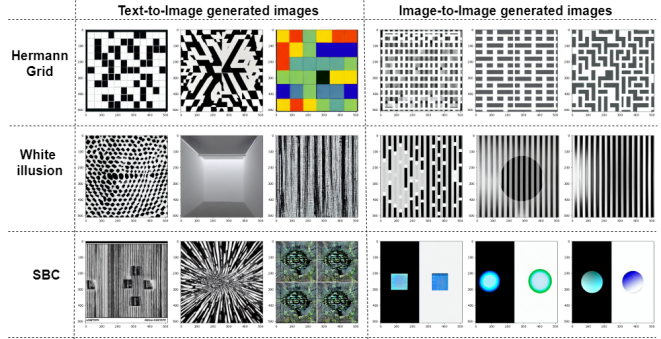


Fig. 6. Diffusion model generated illusion images.

the five classes (White, Hermann grid, grid illusion, SBC, and grating illusion). We consider 500 images from each class for training and test on the remaining images. The results are shown in Tab. 4.

2. Illusion localization. We consider the UNet [14] for illusion localization. We consider 13419 images for training and test on remaining 8947 images. A convex combination of MSE and SSIM loss is used to train the network. We consider various values of the parameters α and β and observe that the best segmentation performance is achieved when $\alpha = 0.4$ and $\beta = 0.6$, i.e., $L = 0.4L_{MSE} + 0.6L_{SSIM}$. The results are shown in Table. 5 where we achieve 84.37% accuracy and a mIoU score of 0.75. Note that $\alpha = 1, \beta = 0$ implies considering the MSE loss, i.e., $L = L_{MSE}$ and $\alpha = 0, \beta = 1$ implies only the SSIM loss, i.e., $L = L_{SSIM}$. The results justify the importance of perceptual cues in the form of SSIM loss for illusion localization.

3. Transition from assimilation illusion to contrast illusion. Here we test the effectiveness of illusion localization while an illusion transition from assimilation to contrast. Note that the model has never seen such transitions. We consider two popular illusion transitions: Howe stimulus [40] and shifted White to checkerboard transition [3].

Howe illusion. Howe illusion [40] is a transition from White illusion to SBC as shown in Fig. 7, where there is a shift of perceived darkness by changing the background. Initially, the leftmost figure in the top row of Fig. 7 is the White illusion. However, as the width of both the dark and white line crossing the patches increases along the row from left to right, the darker patch gets brighter and finally turns into an SBC. The bottom row shows the localization output which is consistent with human observations. Therefore, our learned model can identify such transition in perceived darkness akin to human perception as shown in Fig. 7.

Brightness Transition in Shifted White illusion with Aspect Ratio Variation. Fig. 9 illustrates the shifted White illusion, which is a variant of White illusion [3]. An intriguing feature of shifted White illusion, we found, is the inversion in the perceived brightness/darkness of the patch when we decrease the aspect ratio of the strips as shown in Fig. 9. In the leftmost figure in the top row (Fig. 9) the right patch appears

Table 2. Test accuracy of illusion identification.

Network	Accuracy	F1-score	Precision	Recall
ResNet-18	0.9956	0.9948	1.00	0.9897
AlexNet	0.9973	0.9969	0.9938	1.00
SqueezeNet	0.9956	0.9948	1.00	0.9897

Table 3. Illusion classification using diffusion model generated images.

Method	Accuracy
T2I only	37.85%
I2I only	87.67%
T2I+I2I	81.32%

Table 4. Test accuracy for illusion classification.

Network	Accuracy	F1-score	Precision	Recall
ResNet-18	0.9568	0.9964	0.9995	0.9934
AlexNet	0.8952	0.9455	1.00	0.8967
SqueezeNet	0.9310	0.9738	1.00	0.9490

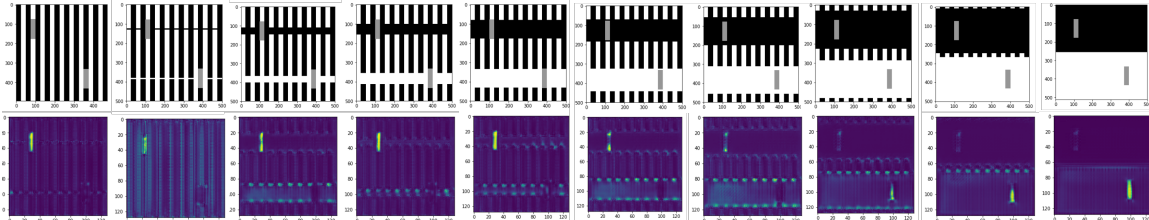


Fig. 7. Howe’s Illusion: Transition from White illusion to SBC. For the images in the upper row in particular, the model localizes the upper left test patch as the dark one, which akin to human perception [40] vacillates and finally localizes in the lower right test patch as the dark one.

Table 5. Test accuracy of illusion localization with various combinations of α and β . Recall the loss function is $L = \alpha L_{MSE} + \beta L_{SSIM}$.

α	β	F1-score	mIoU
1	0	0.5666	0.61
0	1	0.3167	0.46
0.5	0.5	0.4386	0.5
0.6	0.4	0.4395	0.53
0.4	0.6	0.7689	0.75

darker. However, if the aspect ratio of the patch is reduced along the row, i.e. as the stimulus shifts from Shifted White to a Checkerboard, then in the rightmost figure the darker patch turns out to be lighter as shown in Fig. 9. Our learned model adequately mimics such inversion of perceived darkness as shown in Fig. 9.

4. Network analysis. We investigate the feature maps learned by CNN models while identifying the illusions. We compute layer-wise attribution using GradCam [41] to analyze what features are encoded across the CNN layers. This approach, for a given target output, computes the contribution of the image regions for the final prediction across the layers. We use the Captum library [42] for computing the layer-wise attributions. We compare the layer-wise attributions of the ResNet model trained on natural images and trained on illusion images. The result for White illusion is shown in Fig. 8. Note that there is a significant difference between the contribution of the image regions across the layers between the network trained with natural images (top row) and illusions (bottom row). We also notice that the lower layers tend to focus on low-level illusory features such as the boundary between two regions with various intensities. The top layers learn more abstract features. The differences between models trained with natural images and illusions are more prominent in the lower layers. These observations indicate that perception of brightness illusions is primarily a low and mid-level vision task.

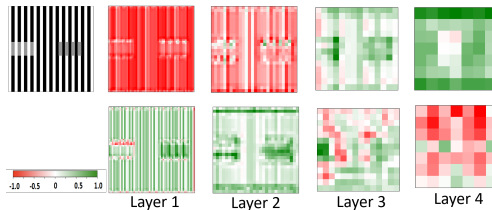


Fig. 8. Gradcam attributes of the ResNet18 layers for the White illusion. Upper row: model trained with natural images using the ImageNet dataset. Lower row: model trained with illusions.

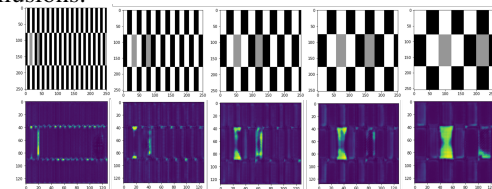


Fig. 9. Transition from assimilation to contrast in Shifted White stimulus: Inversion in perceived darkness is observed by the learned model while reducing the aspect ratio (rightmost image). Images (upper row) and their corresponding response (lower row) by the learned model.

6. CONCLUSION

Understanding and evaluating visual illusions is a challenging task in computational neuroscience. To facilitate exploration in illusion understanding, we have introduced a large-scale dataset of 22,366 images containing five types of brightness illusions. We have annotated each image with the binary mask corresponding to illusory regions in the image. We have validated the dataset by conducting standard psychophysical experiments involving human experts. Next, we benchmark the dataset with deep learning based data-driven approach for illusion identification and localization for brightness illusions. We have conducted extensive experiments evaluating various aspects of our approach.

7. REFERENCES

- [1] Kuntal Ghosh, “A possible role and basis of visual pathway selection in brightness induction.,” *Seeing and perceiving*, vol. 25, no. 2, pp. 179–212, 2012.
- [2] Eric G Heinemann, “Simultaneous brightness induction as a function of inducing-and test-field luminances.,” *Journal of experimental psychology*, vol. 50, no. 2, pp. 89, 1955.
- [3] Michael White, “A new effect of pattern on perceived lightness,” *Perception*, vol. 8, no. 4, pp. 413–416, 1979.
- [4] Ludimar Hermann, “Eine erscheinung simultanen contrastes,” *Pflügers Archiv European Journal of Physiology*, vol. 3, no. 1, pp. 13–15, 1870.
- [5] John M Foley and Mark E McCourt, “Visual grating induction,” *JOSA A*, vol. 2, no. 7, pp. 1220–1230, 1985.
- [6] Frederick AA Kingdom, “Lightness, brightness and transparency: A quarter century of new ideas, captivating demonstrations and unrelenting controversy,” *Vision Research*, vol. 51, no. 7, pp. 652–673, 2011.
- [7] Nikolaus Kriegeskorte, “Deep neural networks: a new framework for modeling biological vision and brain information processing,” *Annual review of vision science*, vol. 1, pp. 417–446, 2015.
- [8] Nobuyuki Otsu, “A threshold selection method from gray-level histograms,” *IEEE transactions on systems, man, and cybernetics*, vol. 9, no. 1, pp. 62–66, 1979.
- [9] Barbara Blakeslee and Mark E McCourt, “A unified theory of brightness contrast and assimilation incorporating oriented multiscale spatial filtering and contrast normalization,” *Vision research*, vol. 44, no. 21, pp. 2483–2503, 2004.
- [10] Alan E Robinson, Paul S Hammon, and Virginia R de Sa, “A filtering model of brightness perception using frequency-specific locally-normalized oriented difference-of-gaussians (flodog),” *Journal of Vision*, vol. 7, no. 9, pp. 237–237, 2007.
- [11] Alan Gilchrist, Christos Kossyfidis, Frederick Bonato, Tiziano Agostini, Joseph Cataliotti, Xiaojun Li, Branka Spehar, Vidal Annan, and Elias Economou, “An anchoring theory of lightness perception.,” *Psychological review*, vol. 106, no. 4, pp. 795, 1999.
- [12] Alexander Gomez-Villa, Adrián Martín, Javier Vazquez-Corral, and Marcelo Bertalmío, “Convolutional neural networks deceived by visual illusions,” *arXiv preprint arXiv:1811.10565*, 2018.
- [13] Kaiming He, Xiangyu Zhang, Shaoqing Ren, and Jian Sun, “Deep residual learning for image recognition,” in *Proceedings of the IEEE conference on computer vision and pattern recognition*, 2016, pp. 770–778.
- [14] Olaf Ronneberger, Philipp Fischer, and Thomas Brox, “U-net: Convolutional networks for biomedical image segmentation,” in *International Conference on Medical image computing and computer-assisted intervention*. Springer, 2015, pp. 234–241.
- [15] Paul Whittle, “Brightness, discriminability and the “crispning effect”,” *Vision research*, vol. 32, no. 8, pp. 1493–1507, 1992.
- [16] Valero Laparra and Jesús Malo, “Visual aftereffects and sensory nonlinearities from a single statistical framework,” *Frontiers in human neuroscience*, vol. 9, pp. 557, 2015.
- [17] Hedva Spitzer and Yuval Barkan, “Computational adaptation model and its predictions for color induction of first and second orders,” *Vision Research*, vol. 45, no. 27, pp. 3323–3342, 2005.
- [18] Eric R Kandel, James H Schwartz, Thomas M Jessell, Department of Biochemistry, Molecular Biophysics Thomas Jessell, Steven Siegelbaum, and AJ Hudspeth, *Principles of neural science*, vol. 4, McGraw-hill New York, 2000.
- [19] Xavier Otazu, C Alejandro Parraga, and Maria Vanrell, “Toward a unified chromatic induction model,” *Journal of Vision*, vol. 10, no. 12, pp. 5–5, 2010.
- [20] Xavier Otazu, Maria Vanrell, and C Alejandro Párraga, “Multiresolution wavelet framework models brightness induction effects,” *Vision research*, vol. 48, no. 5, pp. 733–751, 2008.
- [21] Marina Martinez-Garcia, Marcelo Bertalmío, and Jesús Malo, “In praise of artifice reloaded: Caution with natural image databases in modeling vision,” *Frontiers in neuroscience*, vol. 13, pp. 8, 2019.
- [22] Been Kim, Emily Reif, Martin Wattenberg, Samy Bengio, and Michael C Mozer, “Neural networks trained on natural scenes exhibit gestalt closure,” *arXiv preprint ArXiv:1903.01069 [Cs, Stat]*, 2020.
- [23] Ari S Benjamin, Cheng Qiu, Ling-Qi Zhang, Konrad P Kording, and Alan A Stocker, “Shared visual illusions between humans and artificial neural networks,” in *Proceedings of the Annual Conference of Cognitive Computational Neuroscience*. Available online at: <https://ccneuro.org/2019/proceedings/0000585.pdf>, 2019.

- [24] Emily J Ward, “Exploring perceptual illusions in deep neural networks,” *bioRxiv*, p. 687905, 2019.
- [25] Drew Linsley, Junkyung Kim, Alekh Ashok, and Thomas Serre, “Recurrent neural circuits for contour detection,” *arXiv preprint arXiv:2010.15314*, 2020.
- [26] Eiji Watanabe, Akiyoshi Kitaoka, Kiwako Sakamoto, Masaki Yasugi, and Kenta Tanaka, “Illusory motion reproduced by deep neural networks trained for prediction,” *Frontiers in psychology*, vol. 9, pp. 345, 2018.
- [27] Alexander Gomez-Villa, Adrian Martín, Javier Vazquez-Corral, Jesús Malo, and Marcelo Bertalmío, “Synthesizing visual illusions using generative adversarial networks,” *arXiv preprint arXiv:1911.09599*, 2019.
- [28] Robert Max Williams and Roman V Yampolskiy, “Optical illusions images dataset,” *arXiv preprint arXiv:1810.00415*, vol. 2, 2018.
- [29] Elad Hirsch and Ayellet Tal, “Color visual illusions: A statistics-based computational model,” *Advances in neural information processing systems*, vol. 33, pp. 9447–9458, 2020.
- [30] János Geier, László Bernáth, Mariann Hudák, and László Séra, “Straightness as the main factor of the hermann grid illusion,” *Perception*, vol. 37, no. 5, pp. 651–665, 2008.
- [31] Ashish Bakshi and Kuntal Ghosh, “Tiny squares at the hermann grid corners can completely remove the illusion,” *Perception*, vol. 49, no. 2, pp. 232–239, 2020.
- [32] Soma Mitra, Debasis Mazumdar, Kuntal Ghosh, and Kamales Bhaumik, “An adaptive scale gaussian filter to explain white’s illusion from the viewpoint of lightness assimilation for a large range of variation in spatial frequency of the grating and aspect ratio of the targets,” *PeerJ*, vol. 6, pp. e5626, 2018.
- [33] Veronica Shi, Jie Cui, Xoana G Troncoso, Stephen L Macknik, and Susana Martinez-Conde, “Effect of stimulus width on simultaneous contrast,” *PeerJ*, vol. 1, pp. e146, 2013.
- [34] Alex Krizhevsky, Ilya Sutskever, and Geoffrey E Hinton, “Imagenet classification with deep convolutional neural networks,” *Advances in neural information processing systems*, vol. 25, pp. 1097–1105, 2012.
- [35] Forrest N Iandola, Song Han, Matthew W Moskewicz, Khalid Ashraf, William J Dally, and Kurt Keutzer, “Squeezenet: Alexnet-level accuracy with 50x fewer parameters and < 0.5 mb model size,” *arXiv preprint arXiv:1602.07360*, 2016.
- [36] Zhou Wang, Alan C Bovik, Hamid R Sheikh, and Eero P Simoncelli, “Image quality assessment: from error visibility to structural similarity,” *IEEE transactions on image processing*, vol. 13, no. 4, pp. 600–612, 2004.
- [37] Hang Zhao, Orazio Gallo, Iuri Frosio, and Jan Kautz, “Loss functions for image restoration with neural networks,” *IEEE Transactions on Computational Imaging*, vol. 3, no. 1, pp. 47–57, 2016.
- [38] Robin Rombach, Andreas Blattmann, Dominik Lorenz, Patrick Esser, and Björn Ommer, “High-resolution image synthesis with latent diffusion models,” in *Proceedings of the IEEE/CVF Conference on Computer Vision and Pattern Recognition*, 2022, pp. 10684–10695.
- [39] Chenlin Meng, Yang Song, Jiaming Song, Jiajun Wu, Jun-Yan Zhu, and Stefano Ermon, “Sdedit: Image synthesis and editing with stochastic differential equations,” *arXiv preprint arXiv:2108.01073*, 2021.
- [40] PD Howe, “A comment on the anderson (1997), the todorović (1997), and the ross and pessoas (2000) explanations of white’s effect.,” *Perception*, vol. 30, no. 8, pp. 1023, 2001.
- [41] Ramprasaath R Selvaraju, Michael Cogswell, Abhishek Das, Ramakrishna Vedantam, Devi Parikh, and Dhruv Batra, “Grad-cam: Visual explanations from deep networks via gradient-based localization,” in *Proceedings of the IEEE international conference on computer vision*, 2017, pp. 618–626.
- [42] Narine Kokhlikyan, Vivek Miglani, Miguel Martin, Edward Wang, Bilal Alsallakh, Jonathan Reynolds, Alexander Melnikov, Natalia Kliushkina, Carlos Araya, Siqi Yan, et al., “Captum: A unified and generic model interpretability library for pytorch,” *arXiv preprint arXiv:2009.07896*, 2020.
- [43] G Fechner, “1966,” *Elements of psychophysics*, vol. 1, 1860.
- [44] Paola Bressan, “Explaining lightness illusions,” *Perception*, vol. 30, no. 9, pp. 1031–1046, 2001.
- [45] Leo Poom, “Influences of orientation on the ponzo, contrast, and craik-o’brien-cornsweet illusions,” *Attention, Perception, & Psychophysics*, vol. 82, no. 4, pp. 1896–1911, 2020.
- [46] Dejan Todorović, “Lightness and junctions,” *Perception*, vol. 26, no. 4, pp. 379–394, 1997.
- [47] Alan Gilchrist, “A gestalt account of lightness illusions,” *Perception*, vol. 43, no. 9, pp. 881–895, 2014.

- [48] Christopher E Buckle, Viyan Udawatta, and Christopher M Straus, “Now you see it, now you don’t: visual illusions in radiology,” *Radiographics*, vol. 33, no. 7, pp. 2087–2102, 2013.
- [49] Li Fei-Fei, Rob Fergus, and Pietro Perona, “Learning generative visual models from few training examples: An incremental bayesian approach tested on 101 object categories,” in *2004 conference on computer vision and pattern recognition workshop*. IEEE, 2004, pp. 178–178.
- [50] Barbara Blakeslee and Mark E McCourt, “When is spatial filtering enough? investigation of brightness and lightness perception in stimuli containing a visible illumination component,” *Vision Research*, vol. 60, pp. 40–50, 2012.

8. SUPPLEMENTARY MATERIAL

In the supplementary material, we are providing the following details.

1. Dataset curation details
2. Details of psychophysical experiments and results.
3. Details of dataset generation.
4. Networks details for illusion detection and localization.
5. More qualitative experimental results.
6. Generalization to unseen illusions.
7. Illusion vs natural images.
8. Test on illusions in natural images.
9. Network analysis.

9. DATASET CURATION DETAILS

Our dataset and code can be downloaded from the public domain <https://github.com/aniket004/BRI3L>. More details of dataset maintenance, download and usage have been provided in this website. A simple evaluation of the methods using the dataset can be evaluated using the google colab notebook: notebook

10. PSYCHOPHYSICAL EXPERIMENT : DETAIL EXPERIMENTAL SETUP, PROCEDURE AND RESULT.

10.1. Background

Gustav Theodor Fechner [43] was the pioneer to set the principles and procedures of psychophysics. It is a sub-discipline of psychology and deals with the relationship between physical stimuli and their subjective correlates or percepts. In different intensity based visual illusions, the lightness of the test patch is modified which is termed as illusory effect. This illusory effect is subjective in nature. Performing comparison of the intensity of the test patch with a standard patch of known intensity, one can only guess whether the test patch is lighter or darker as compared with the standard. Psychophysical experiments are designed to measure the illusory effect quantitatively and can also judge the direction of the illusory effect.

A psychophysical experiment consists of a number of components like stimulus (comparator and standard), task, method, analysis and measure. Two types of procedures exist in psychophysical experiments. In the first type, the comparator is displayed on the computer screen and the observer has to adjust the contrast within a predefined limit to achieve the perceivable intensity as compared with the standard. For this type of procedure, the task and the method are collectively

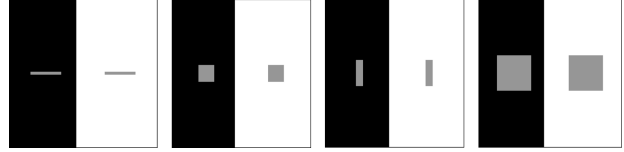


Fig. 10. Different types of SBC illusions selected as the comparator. The intensity level of the target is always 150. However the length and width of the target varies widely.

termed as ‘method of adjustment’. Nowadays the preferred approach is to display the comparator and standard in a random fashion on a computer screen for a short duration of time. The observer has to decide the relative brightness of the comparator with respect to that of the standard and indicate his/her choice by pressing a key. This is known as 2 Alternate Forced Choice (2AFC) experiment [32].

Four types of intensity based illusions namely, Simultaneous Brightness Contrast(SBC), White Illusion (WI), Gratings and Lower Grid illusions with variable parameters (say length, width, intensity background etc.) are generated randomly and the darker patch is selected as the target patch or comparator. The two alternate forced choice (2AFC) experimental setup has been adopted to quantify the illusory enhancement or reduction of the selected target patch. The psychometric curve is drawn in Fig. 4 (in the paper) and Fig. 11 for a specific illusion and the illusory effect of the test patch is quantified at the point of subjective equality (PSE).

10.2. Materials and Methods

The experimental arrangements are designed identical to that described in Mitra et al. [32] and Shi et al. [33]. A chin rest is placed at a distance of d cm from a linearized video monitor (HP Compaq LE 2002X with resolution 1,024 X 1,024 pixels) and the subject’s head is stabilized on this chin rest. The value of d is chosen as 57 cm, because it may be shown from simple trigonometry that at such a distance an image of width (or length) of one cm. subtends a visual angle of approximately 1 degree. Subjects binocularly view the visual presentations, keeping their heads fixed on the chin rest. In these experiments, the subjects visually compare the brightness or lightness of two targets, namely the standard and the comparator. We conduct a two-alternative forced-choice experiment for lightness discrimination between the comparator and the standard and measured the illusory enhancement or illusory reduction. The subjects are instructed to give his/her judgment by pressing the key marked ONE when the comparator appeared to be lighter than the standard, otherwise key marked as TWO was to be pressed. The comparator is an intensity based illusion generated statistically and it is selected individually from four types of illusions namely Simultaneous Brightness Contrast (SBC), White Illusion (WI), Gratings and Lower Grid illusions. In one set of experiment, the same

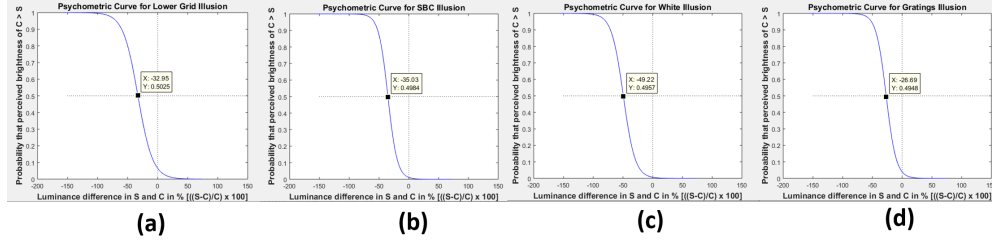


Fig. 11. Psychometric curve for (a) Lower grid, (b) SBC, (c) White illusion, (d) Grating illusion taken from the generated dataset. This indicates the probability that the perception agrees with the reality as a function of the real difference in luminance between the standard (S) and the comparator (C). The illusory reduction for Grating, White illusion, SBC, Lower grid are 26.69, 49.22, 35.03 and 32.95 respectively.

type of the illusion, say SBC illusion is selected as the comparator. One such set of SBC illusion is shown in Fig. 10. The intensity level of the target remains always 150, however it appears either lighter or, darker depending on the background intensity. In all the trials, the darker target is selected as the comparator, whose intensity is compared with the standard.

In our experiments, the standard is a target, containing a number of segments. Each segment could be distinguished from the other by its intensity of gray value. For example, our striped standard was divided into 11 segments of varying intensity values values 13, 36, 59, 82, 105, 128, 150, 173, 196, 219 and 242. These values are kept fixed during the entire experiment, although the order of appearance of these 11 segments within the standard are scrambled pseudo-randomly. So the appearance of the standard varies from trial to trial.

The screen design for two-alternate forced-choice experiment is shown in Fig. 6 (in the paper) for White illusion and SBC respectively. In each trial, the subject has been first instructed to fix attention on a central red cross (1 deg within a 3.5 deg fixation window). Within one second the comparator and standard appears on the screen simultaneously, one of them centered at 7 deg to the left of the red cross and the other centered at 7 deg to the right of the red cross. Two vertical red lines are introduced on the comparator and standard at the same height of the red cross, which denotes the specific area of interest of them to be compared. The comparator and standard exists on the computer screen for about 3 seconds before disappearing. Subjects need not had to wait to give their judgments till the stimuli disappeared from the display. Red lines indicate the region of interest in the comparator to be judged against the nearest segment of the standard. If the comparator appears to be lighter than the standard, subjects have to press key number ONE, otherwise they have to press key number TWO. During one set of experiment (say for Simultaneous Brightness Contrast illusion), both the comparator (varying its width and length) and standard (by scrambling 11 intensity levels) are changed from trial to trial.

The perceived difference of brightness between the comparator and standard depends on the actual difference of

brightness and also on the psychophysical response of the subject. To keep the subjects unbiased and attentive, various parameters were changed randomly from trial to trial. As an example, we can state that the comparator can appear to the left or right of the red cross, the intensity of the standard appearing at the same height of the comparator can vary widely etc. Perceived difference of brightness between the comparator and the standard depends on the actual difference of brightness between those and also the psychophysical effect on the subject. If the actual difference in the brightness of the co-occurring comparator and the standard is zero, the apparent perceived difference is then entirely due to the psychophysical effect.

10.3. Experimental Results

The purpose of psychophysical experiment is to measure *Point of Subjective Equality* (PSE) [32], which is a measure involving actual intensities of the comparator and standard, when these appear to be same to the subject. In our experiments, the illusory enhancement or illusory decrement are measured at the point of subjective equality from the different sets of psychometric curves drawn for four different illusions. As always we measure the illusory effect of the darker target, we can calculate the average illusory decrement for each type of illusion under consideration.

Two sets of psychometric curves are presented in the paper. They represent the psychometric curves for Simultaneous Brightness Contrast (SBC) illusion and White illusion. We have performed similar experiments for other variants of illusions present in the dataset. The psychometric curves for SBC, White illusion, gratings illusion and lower grid illusion are provided in Fig. 11. Illusory decrement indicates the quantitative measure of perceived darkness. For example, given the standard grayscale value to be 150, illusory reduction of 32.95 indicates that the target is perceived to be grayscale value of 117.05 and looks darker. The illusory reduction of the same intensity comparator of grayscale value 150 for White illusion is maximum (49.22), for gratings illusion is minimum (27.11), and it lies within this maximum

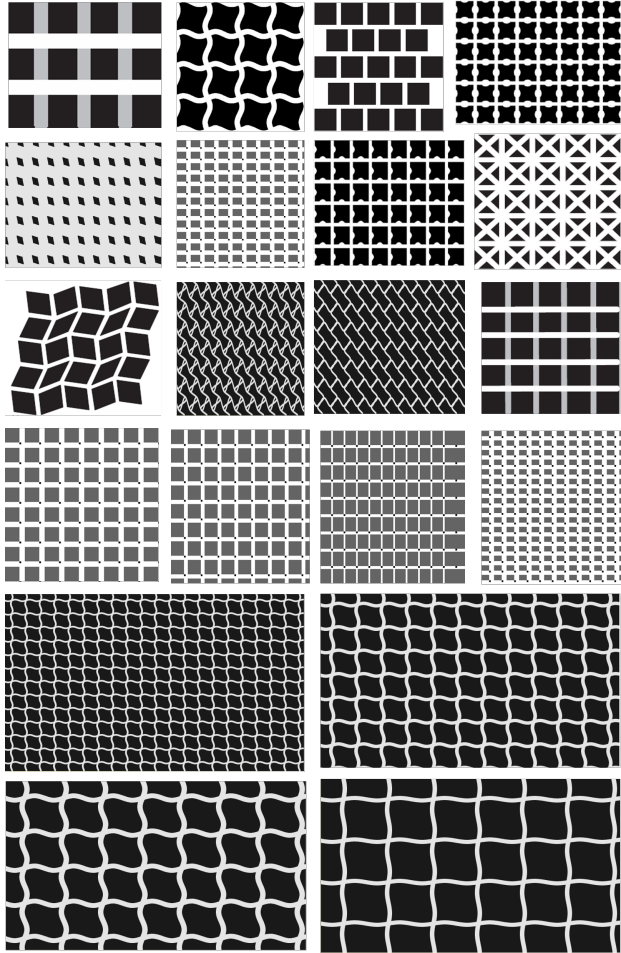


Fig. 14. Non-illusion examples generated by us in the dataset by introducing non-linearity, dot-insertion [31, 30] etc.

calization using transposed convolutions. The exact architecture is shown in Fig. 12. The experimental details are given in Table 3 (in the main paper). We consider a weighted combination of MSE loss (L_{MSE} and SSIM loss (L_{SSIM}) as the loss function, $L = \alpha L_{MSE} + \beta L_{SSIM}$, where L_{MSE} is mean squared error loss and L_{SSIM} [37] is the SSIM loss. We experimentally set the parameters, $\alpha = 0.4$, $\beta = 0.6$, which produced the best performance as shown in Tab.3 (in the main paper). Adam optimizer is used for training with batch size of 32 and a learning rate of 0.001. Some of the qualitative results on test images are shown in Fig. 15.

13. QUALITATIVE RESULTS ON UNSEEN ILLUSIONS

In this section, we verify the efficacy of our proposed data-driven approach on some more well-known illusions, which have not been used during training. Qualitative network response for variants of dungeon illusion [44] (Fig. 20), SBC

Illusion	Accuracy	mIoU
Hermann grid	0.6905	0.43
Induced grating	0.9206	0.49
Lower grid	0.7991	0.43
Upper grid	0.8546	0.44
SBC	0.8805	0.48
White	0.9745	0.5

Table 6. Transferring illusions across other brightness illusions: testing on particular illusion as mentioned in the rows (from our dataset) while training the segmentation model for dark region localization on all other types except that particular illusion.

with luminance gradient [45] (Fig. 16), criss-cross brightness illusion [44](Fig. 17), Todorovic illusion [46](Fig. 18), benary’s cross [47] (Fig. 21) and cornsweet illusion [45] (Fig. 19) are shown here. These results suggest that the trained model can also correctly predict the perceived darkness on these type of unseen illusions.

14. GENERALIZATION TO UNSEEN ILLUSIONS.

To check whether the learned model generalizes among brightness illusions, we perform the following experiment. Among the five types of illusions, we train a segmentation network on four types of illusions and test on the unseen one. We show the results in Table. 6. For example, we train on all the illusion images except the Hermann grid and test its generalization performance on the Hermann grid and observed illusion localization accuracy of 69.05% with mIoU of 0.43 as shown in Table. 6. We find that the learned segmentation model generalizes poorly when testing on the Hermann grid. However, for all other cases, the trained model transfers quite effectively for the other four types of illusions as shown in Table. 6. We believe, as in the Herman grid, the illusory regions are not physically present and thus make the localization challenging.

Beyond these five types of illusion, we also evaluate of other popular unseen illusions such as Mach band illusion, non-linear Hermann grid, and Dungeon illusion.

Mach band illusion. Mach bands are apparent bright and dark lines occurring at the border between objects with different optical densities, contrast levels, or luminances [48]. Fig. 22 indicates that our learned model can detect Mach bands. Note, since we have trained to identify the darker patch, the learned model can identify the bright Mach band by displaying two surrounding parallel darker regions as shown in Fig. 22.

15. ILLUSION VS NATURAL IMAGE.

We test illusion vs natural image (from the Caltech101 dataset [49]) classification and achieve a high test accuracy of 99.98 % in only 5 epochs.

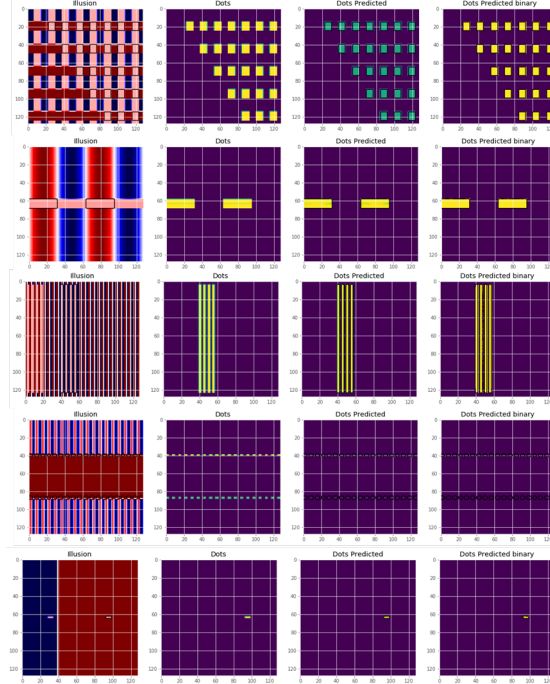


Fig. 15. Network response for illusion localization on test set: (a) test images, (b) corresponding groundtruth, (c) network response, (d) Binary response of the network by thresholding at 0.22. The trained network can localize perceived darkness quite efficiently.

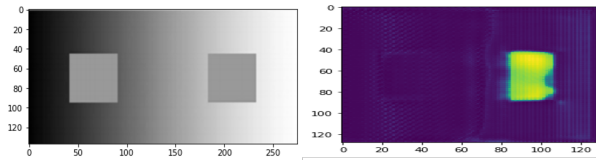


Fig. 16. Network response for SBC with luminance gradient: illusion image (left), network response (right). Instead of binary background in SBC, the background has luminance gradient. The model still identifies the darker patch.

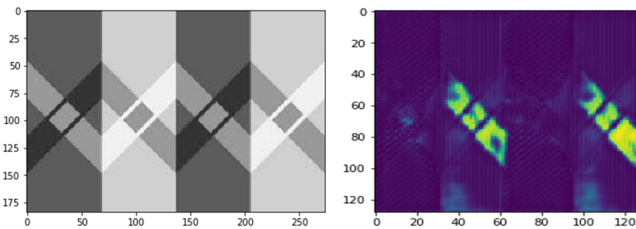


Fig. 17. Network response for criss-cross brightness illusion: illusion image (left), network response (right). The darker patches are identified by the model.

16. TEST ON ILLUSIONS IN NATURAL IMAGES.

We test on natural images with diverse lighting and shading information which are used in illusion studies, e.g., Cartier-Bresson stimulus, as shown in Fig. 24 [50]. Our model can identify the darker regions and Mach bands in natural images as shown in Fig. 24. We have also tested our framework with some of the recent approach of generating illusions from natural images [29]. Fig. 24(d) shows that our approach can identify illusory regions in those generated illusions too.

17. NETWORK ANALYSIS

We investigate the feature maps learned by CNN models while identifying the illusions. We compute layer-wise attribution using GradCam [41] to analyze what features are encoded across the CNN layers. This approach, for a given target output, computes the contribution of the image regions for the final prediction across the layers. We use the Captum library [42] for computing the layer-wise attributions. We compare the layer-wise attributions of the ResNet model trained on natural images and trained on illusion images.

In addition to the Gradcam attributes provided in the main paper, we are also providing some more examples of layer wise gradcam attributes for Hermann grid, SBC, non-illusion variant of Hermann grid and lower grid illusion in Fig. 25, Fig. 26, Fig. 27 and Fig. 28 respectively. As indicated in the

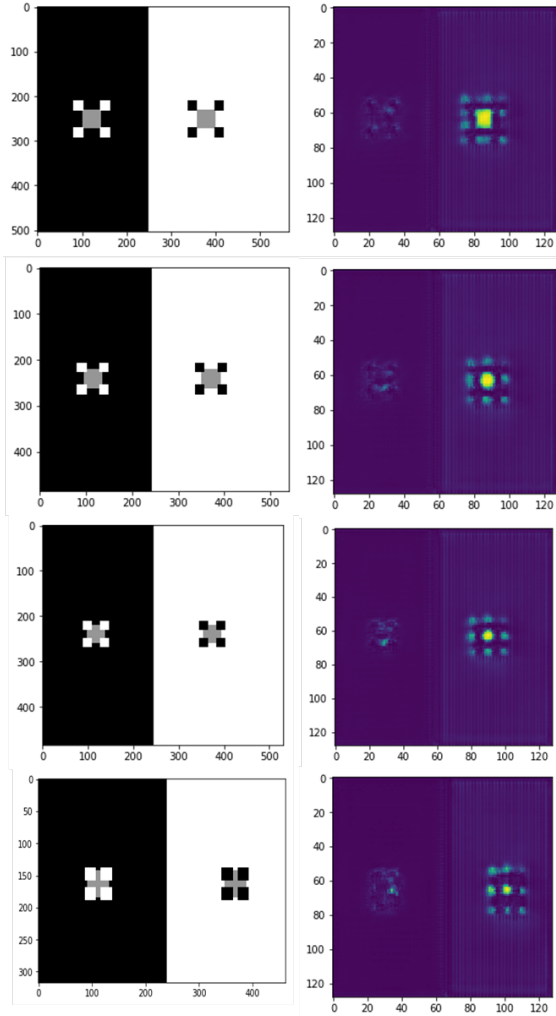


Fig. 18. Network response for todorovic illusion: todorovic illusion (left), network response (right). As the gray patch occludes by surrounding, the illusory effect is more focused in the center.

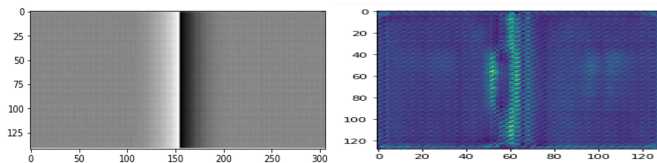


Fig. 19. Network response for cornsweet illusion: cornsweet illusion (left), network response (right). The model correctly identifies the darker patch at the right.

main paper, there is a significant difference between the contribution of the image regions across the layers between the network trained with natural images (top row) and illusions (bottom row).

In these examples also the lower layers tend to focus on

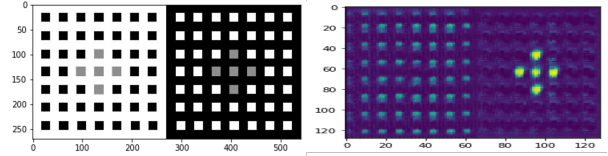


Fig. 20. Network response for dungeon illusion: dungeon illusion (left), network response (right). The gray patches in the right looks darker, which the model correctly predicts. It also predicts Hermann grid blobs in the left side.

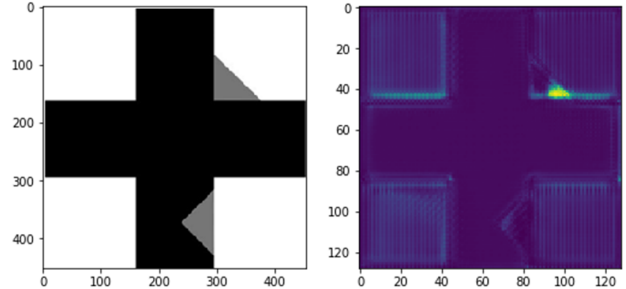


Fig. 21. Network response for Benary's cross: Benary's cross (left), network response (right). The upper right gray patch seems to look darker, which the model correctly predicts.

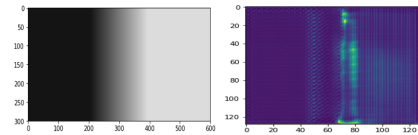


Fig. 22. Mach band illusion (left) and corresponding learned model output (right). Two dark parallel dark patch indicates Mach band.

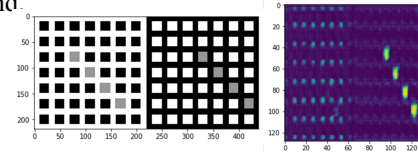


Fig. 23. Dungeon illusion and corresponding response from the network: Right region seems to be darker than left ones, however they are exactly the same grayscale level.

low-level illusory features such as boundary between two regions with various intensities and the top layers learn more abstract features. The difference between the models trained with natural images and illusions are more prominent in the lower layers.

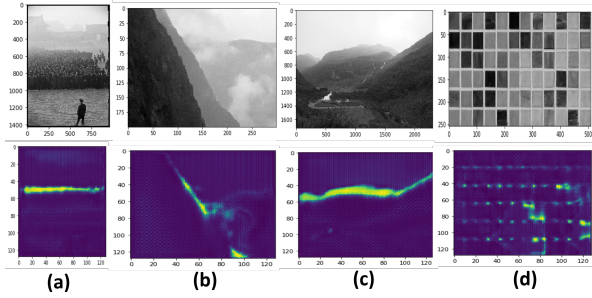


Fig. 24. Model response (lower row) on natural images (upper row): (a), (b), (c) natural images showing Mach band, (d) Illusory regions identified in illusions generated from natural image by [29].

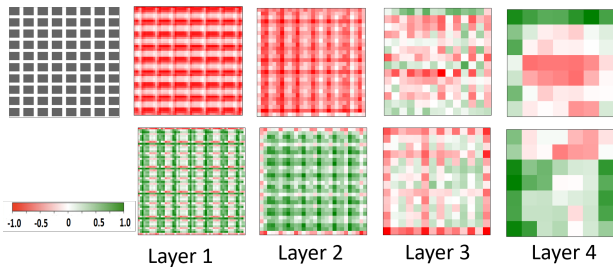


Fig. 25. Gradcam attributes of the ResNet18 layers for the Hermann grid illusion. Upper row: model trained with natural images using the ImageNet dataset. Lower row: model trained with illusions. The layer attributes are clearly different for both these cases. Also, illusion finetuned model seems to capture the darker regions or patches in the lower layer response.

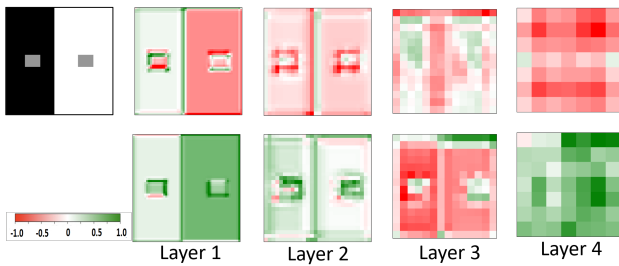


Fig. 26. Gradcam attributes of the ResNet18 layers for SBC. Upper row: model trained with natural images using the ImageNet dataset. Lower row: model trained with illusions. The layer attributes are clearly different for both these cases. Also, illusion finetuned model seems to capture the darker regions or patches in the lower layer response.

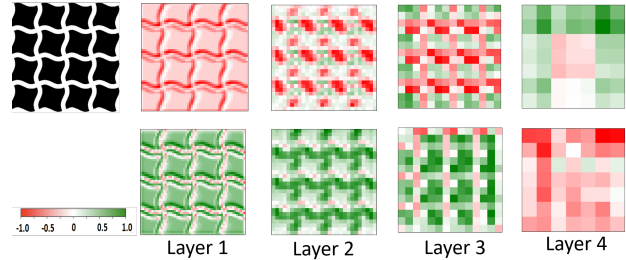


Fig. 27. Gradcam attributes of the ResNet18 layers for the non-illusion variant of Hermann grid. Upper row: model trained with natural images using the ImageNet dataset. Lower row: model trained with illusions.

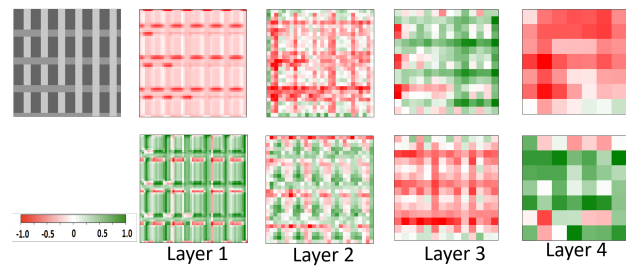


Fig. 28. Gradcam attributes of the ResNet18 layers for lower grid illusion. Upper row: model trained with natural images using the ImageNet dataset. Lower row: model trained with illusions.